

Application of discrete modelling approach to yeast drying.

F. Debaste,^a and V. Halloin^a

^a*Chemical engineering department, Université Libre de Bruxelles Av. Franklin Roosevelt, 50 CP
165/67 B-1050 Brussels, Belgium*

Abstract

Yeast drying is widely used to ease transport and conservation. In this work, Baker's yeast drying in fluidized bed is modeled using of pore network model. Classical balances equations at the reactor scale are coupled with the pore network for the grain, which takes into account diffusion in the gas phase, transport by liquid film in partially saturated region and pressure gradient effects in the liquid phase. Porous structure to be applied in the model is obtained using environmental scanning electron microscope. Simulations are validated on a thermogravimetry analysis experiment. Model is then applied for fluidized bed drying for which experimental results obtained on laboratory pilot are available. Finally, the results of the model are compared to those of a simplified receding front model.

Keywords: yeast drying, fluidised bed, discrete model, pore network model.

1. Introduction

Drying of yeast is of major importance for food industry. Transport and shelf life of yeast are highly dependant on the drying process (Bayrock and Ingledew, 1997b). This step is highly energy consuming and can alter product quality. For yeast, crucial question is the viability of the cells. It is affected by the complete drying conditions : temperature, heat fluxes, humidity, speed of drying can all be of critical importance (Chen and Patel, 2007). Therefore, physical modelling of the process of yeast drying is particularly useful. It allows enhanced understanding of the conditions to which yeast is exposed.

Classical models of yeast drying are based on desorption isotherms: experimental curves of equilibrium solid moisture content as a function of air moisture content. Such models have several limitations :

1. obtaining experimental desorption isotherms is a difficult and expensive process. Moreover, the isotherm depends on solid geometry. So if yeast grains are modified, in theory, the isotherm measurements have to be repeated.
2. models are very sensitive to isotherms. Hence, a precise model would require a very precise isotherm, which cannot always be obtained experimentally.

3. although isotherms are based on equilibrium, they are often used to model the kinetic of the drying; some kinetics effect cannot be highlighted by such a method.

In this approach, falling rate period is correlated to the evaporation of bounded water (Bayrock and Ingledeew, 1997a). It is widely known in drying that this period can be attributed to many different phenomena (Bear and Buchlin, 1991). Recent modelling for the drying of granulated yeast insists on the influence of transport phenomena inside the granules (Türker *et al.* 2006).

Most non-isotherm based models integrating the effect of solid structure on drying are based on a continuum approach. The porous system is modelled by a fictive continuous medium (Whitaker, 1977).

In this paper, a discrete modelling of yeast grain is tested. The medium is modelled directly at the pore scale by considering a network of pores linked together by throats. Simplified local transport equations for each throat and pore are then solved. Such models naturally take into account phenomena that classical models can't easily handled as the fractal form of the drying front. This represents a powerful complementary tool to continuous approach (Sahimi, 1993). Network parameters of the models are deduced from the analysis of the solid structure observed with an environmental scanning electron microscope.

The model is validated by comparison with experiments of drying of a small quantity of yeast in a thermogravimetry analyzer (TGA). The practical case of fluidized bed drying is then studied. The simulations couple the pore network model for yeast grains to classical transport equations for the whole reactor. The results are compared to experimental data on a laboratory pilot plant and to a simple receding front continuous model. This comparison highlights strengths, weaknesses and complementarities of both modeling approaches.

2. Methods and materials

2.1. TGA experiment

TGA offers the opportunity to have precise and simultaneous measurement of weight and temperature for a sample exposed to controlled gas and heat fluxes. Placing a small amount of yeast in a dry air flow at constant temperature allows the reproduction of a simplified drying process.

The experiment is realized using a Mettler Toledo TGA/SDTA851e. 40 mg of ungranulated *Saccharomyces Cerevisiae* are exposed to dry air at 36° C at a rate of 30 ml/min. Experimental cell is 6 mm of diameter and 1,6 mm deep. Measurements are realized every 72 seconds. Figure 1 presents the observed mass, mass loss and temperature. Only the first 10000 seconds are shown of the figure because all evolution happens within this period but experiment is carried out for a total period of 36000 seconds to verify the absence of later evolution.

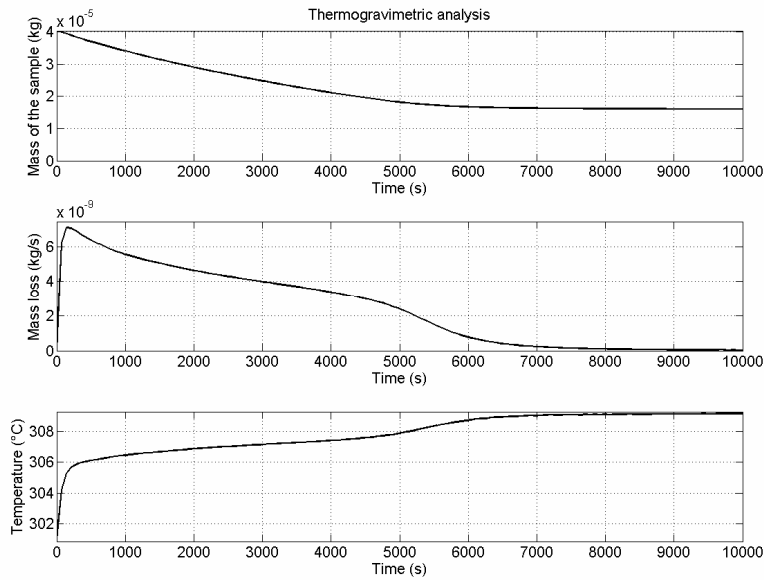


Figure 1 : Results of the TGA analysis. The abscise presents the time evolved since the beginning of the experiment. From top to bottom total mass, mass loss and temperature are presented.

Three distinct periods can be observed on drying rate and temperature graphs :

1. a transient starting zone in the 200 first seconds,
2. a first falling rate period until 5000 seconds,
3. a second faster decreasing falling rate period.

2.2. Fluidized bed drying

Batch yeast drying experiments are performed in a laboratory scale fluidized bed dryer designed and constructed in the chemical engineering department of the Faculty of Applied Sciences, ULB. Details of the experiments can be found elsewhere (Bossart, 2006; Debaste *et al.*, 2007). A typical experimental result is presented in Figure 2. The curves present the change with drying time of the solid moisture content and air humidity and temperature at the exit of the fluidized bed.

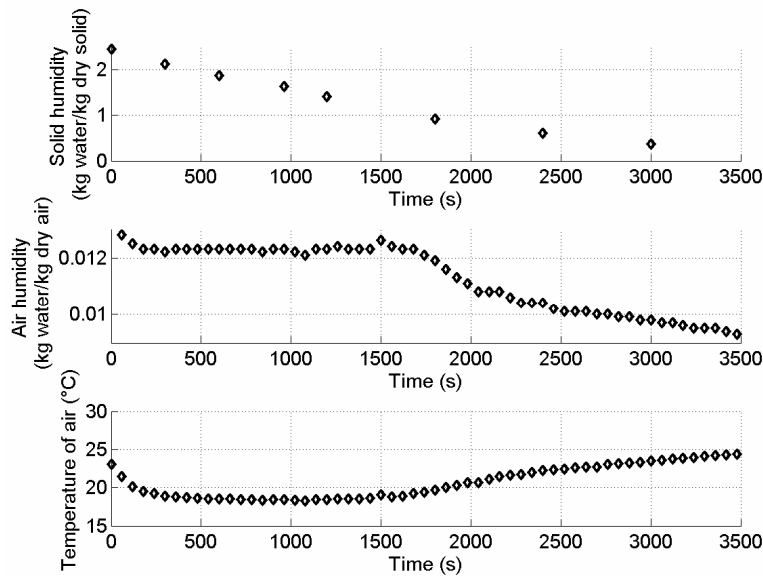


Figure 2 : Typical fluidized bed drying curve. The abscise presents the time evolved since the beginning of the experiment. From top to bottom total sample mass, outlet air humidity and outlet air temperature are presented.

As in the TGA experiment, three well-identified zones are visible:

1. a first transient starting zone,
2. the drying constant rate zone and
3. a drying falling rate zone.

As expected, the boundaries between zones are located at the same drying times on temperature and humidity curves.

2.3. Porous network model

In this section, porous network models for evaporation are briefly presented. Equations details can be found, amongst others, in the works of Laurindo and Prat (1996, 1998), Prat (1995, 2002) and Yotis *et al.* (2001, 2004).

In the porous network approach, the porous medium is replaced by an idealized network of pores connected to each others by throats. Throats represent passages where flow limitations are observed while the pores represent the places where fluid is stored (Prat, 2002). For evaporation modelling, at a given time, an element, i.e. a pore or a throat, can completely be filled with liquid, gas, or contain both separated by an evaporating interface. Moreover, part of the gas region is supposed to contains wetting films. Theses films are supposed to evaporate at their end and to be continuously fed by the liquid phase, therefore enhancing mass transfer in the medium (Yiotis *et al.*, 2004). Typical 2D system presenting gas, film and liquid regions is illustrated on Figure 3

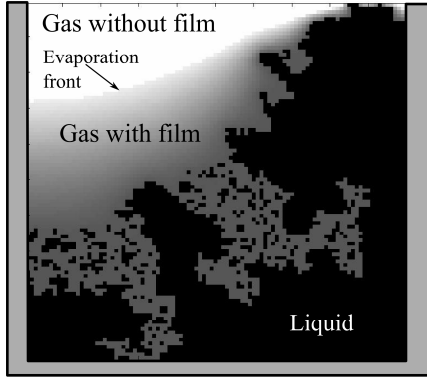


Figure 3 : Illustration of a typical 2D network evaporating from the upper surface. Black correspond to liquid filled regions, gray scales correspond to film thickness and white zone to gas filled region

2.3.1. Mass balance in gas filled region

The model relies on mass balance. In regions filled with gas and where no films are present, diffusion of a dilute vapor in a perfect gas is assumed. Accordingly, diffusion equation is solved (Bird *et al.*, 2002):

$$\frac{DM_v\Omega}{RT}\Delta p_v = 0 \quad (1)$$

Where (see Nomenclature section for units) D is diffusion coefficient, M_v is molecular mass of vapor, R is perfect gas constant, T is temperature, p_v is partial vapor pressure, Ω is the throat cross section and Δ is laplacian operator.

For gas filled regions where films are present, mass transfer is assumed to be dominated by wetting film transport. Mass balance can be written as (Yiotis *et al.*, 2004):

$$\frac{\kappa\rho_l\gamma}{3\mu}\Delta y^3 = 0 \quad (2)$$

Where κ is the hydraulic conductivity coefficient of the films, ρ_l the volumic mass of liquid, μ the viscosity of liquid, γ the interfacial tension of the liquid gas system and y is the film thickness.

Assumption is made that all the film evaporation occurs at the end of film dominated region. Where film is present, gas is supposed to be saturated in vapor. At the interface between film and vapor diffusion dominated region, a one dimensional balance writes as:

$$\frac{DM_v\Omega}{RT}\left(\frac{dp_v}{dx}\right) = \frac{\kappa\rho_l\gamma}{3\mu}\left(\frac{dy^3}{dx}\right) \quad (3)$$

Non-dimensional variables, star labeled, can be introduced. y and x are divided by a specific length \bar{d} chosen here as the square root of the average cross section of a

throat. Partial vapor pressure is divided by saturation pressure P^{sat} . Equation (3) can be rewritten as:

$$\left(\frac{dy^{*3}}{dx^*}\right) = Ca \left(\frac{dp_v^*}{dx^*}\right) \quad (4)$$

Where Ca is called the capillary non-dimensional number, and is defined as

$$Ca = \frac{3\mu DM_v P^{sat}}{RT\kappa\rho_l \bar{\gamma}l} \quad (5)$$

This number compares vapor diffusion transport to film transport.

Introducing a new variable;

$$\Phi = \frac{y^{*3} + (Ca p_v^*)}{1 + Ca} \quad (6)$$

equations (1), (2) and (4) become only one equation describing both regions :

$$\Delta\Phi = 0 \quad (7)$$

After solving this equation, film thickness and vapor pressure can be determined by using equation (6). The boundary between the two sub-domains is given by

$$\Phi = \frac{Ca}{1 + Ca} \quad (8)$$

At the meniscus, where the liquid phase give birth to the film, thickness of the film y_c is assumed to correspond to the thickness it would have at percolation threshold.

At porous medium exit, a diffusive layer of constant thickness δ is assumed.

2.3.2. Mass balance in liquid filled region

For the liquid filled region, mass flow balance is written as

$$\sum_j Q_{ij} = 0 \quad (9)$$

Where Q_{ij} is the flow rate from pore j to pore i and summation is done on all first directly connected neighbors. Expression of Q_{ij} depends on the phase contained by the adjacent pore :

- when filled with liquid, flow rate is expressed as:

$$Q_{ij} = \frac{\rho_l g}{\mu} (p_{lj} - p_{li}) \quad (10)$$

where g is the hydraulic conductance of the throat.

- when the adjacent pore is partially filled with liquid and gas, p_{lj} is replaced by atmospheric pressure p_g , supposing that in the pore, capillary effect are negligible.
- when adjacent pore is fully filled with gas, flow rate correspond to film transport or evaporation from the throat:

$$Q_{ij} = \frac{2\gamma\kappa\rho_l\Omega}{3\mu l} (1 + Ca)(\Phi_j - \Phi_c) \quad (11)$$

with l being the length of the throat.

2.3.3. Algorithm

At the beginning of a simulation, a fully liquid filled network is generated. Figure 4 presents schematically the 7 point algorithm corresponding to one time step :

1. Different clusters, *i.e.* continuous liquid zones, identification.
2. Emptying of throats is considered. Two invasion mechanisms are considered: capillary and viscous invasion. All the throats at the liquid-gas boundary are first checked for viscous emptying: pressures in the two adjacent pores (one filled with liquid, the other with gas) are compared. If pressure difference overrides capillary pressure, the throat is invaded by gas. So, the condition of viscous invasion is written as

$$p_g - p_l > p_c \quad (12)$$

where p_c is the capillary pressure in the throat, given by Laplace equation :

$$p_c = \frac{\gamma}{y_c} \quad (13)$$

For every cluster where no viscous invasion occurs, capillary invasion is considered. The throat presenting the lowest capillary pressure (following equation (13)) in the cluster is emptied.

3. Calculation of the Φ field from equation (7) by discretisation.
4. Computation of liquid pressures from equations (9) to (11).
5. The update of pressure field can induce some throats to fall under the condition of equation (12). Consequently, pressure field modification leads to their invasion. Therefore if such throats are detected, algorithm is brought back to step two. However this time only viscous invasion is tested.
6. When step 5 finally shows no new throat to invade, time to empty interfacial pores is calculated. A mass balance is written for every partially or fully liquid filled pore in contact with gas. Hence, for adjacent pore filled with liquid, equation (10) is used by replacing p_{li} by p_g and for adjacent pore containing gas evaporation rate is computed using equation (11). The net flow rate that is obtained allows the calculation of the time needed to empty the pore.
7. Emptying of the pore that takes the less time to be cleared. The needed time is the time step. The quantity contained in the other pores is updated using the flow rate calculated at point 6.

Iterations are performed until the network doesn't contain any liquid filled pore.

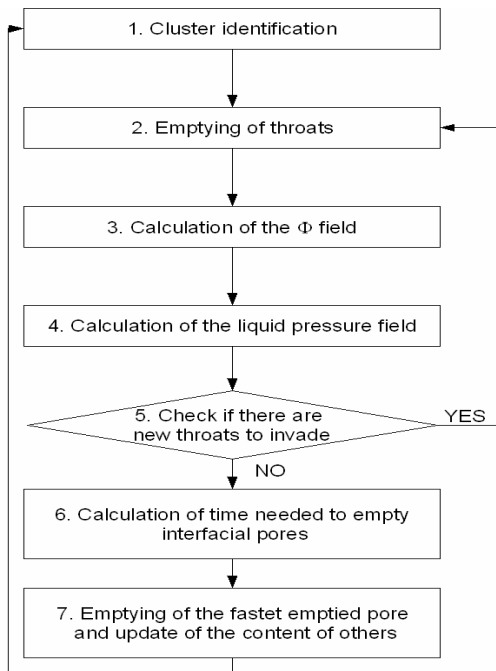


Figure 4 : General presentation of the algorithm of the porous network model.

2.3.4. Coupling with global balance equations

Temperature variations inside the grain are not taken into account. Liquid and solid are supposed to be at a uniform temperature. This temperature is evaluated using a global energy balance in the reactor (TGA cell or fluidized bed) supposed to be perfectly mixed. Because of the small differences of temperature in the system, the terms in the global enthalpy balance including the specific heat of vapor are small compared to the terms including the latent heat of vaporization and the specific heat of air. Therefore, they are neglected in the enthalpy balance.

Accordingly, the global enthalpy balance writes as follows:

$$G(y_{in} - y)\lambda + Gc_{p,g}(T_{in} - T) = m_s(c_{p,s} + c_{p,l}x)\frac{dT}{dt} + m_s c_{p,l}(T - T_{in})\frac{dx}{dt} \quad (14)$$

where G is the external mass flow rate of air, y and y_{in} are humidity of air in the reactor and at the entrance, $c_{p,g}$, $c_{p,s}$, $c_{p,l}$ are heat capacity of gas, solid and liquid, λ is the latent heat of vaporization of water, m_s is the dry solid mass, T_{in} is the temperature of air at the entrance of the reactor and x is the amount of liquid water in the porous medium. $\frac{dx}{dt}$ and x are directly computed by the porous network. Effect of temperature on fluid properties is only taken into account through the saturation pressure of the gas using Clapeyron law.

To model the TGA experiment, no other equations are needed. For the fluidized bed, a mass balance for air humidity over the entire reactor is also considered:

$$m_g \frac{dy}{dt} = G(y_{in} - y) - m_s \frac{dx}{dt} \quad (15)$$

with m_g being the mass of gas in the fluidized bed.

Practically, equations (14) and (15) are discretized using Crank-Nicolson scheme (Versteeg and Malalasekera, 1995). To achieve resolution of this system, porous network time step has to be reduced to comply with numerical needs of the discretized differential equation system. Therefore, at every time step, the pore normally emptied at the point 7. of the algorithm is only partially invaded. Saturation pressure corresponding to the new reactor temperature and reactor air humidity are then updated in the porous network.

2.4. Porous structure analysis and transposition to the model

In this work 2D network is presented, but methodology can be extended to 3D (Le Bray and Prat, 1999). Every pore is supposed to connect to 4 neighbors. Geometrical properties of pores (volume) and throats (specific length d) have statistically distributed values.

Network properties are evaluated based on environmental scanning electron microscope (ESEM) and on mercury porosimetry. A typical yeast grain structure visualised with ESEM is shown on Figure 5. The grain is composed of an aggregation of roughly spherical colonies. Precise analysis of ESEM results and mercury porosimetry show that the spatial arrangement of colonies does not correspond to a dense packing of sphere. Colonies form complex structure characterized by large pore compared to colonies size (Boulton and Quain, 2001). Mean pore radius seems to be around 15 μm while colonies have a typical radius of 5 μm .

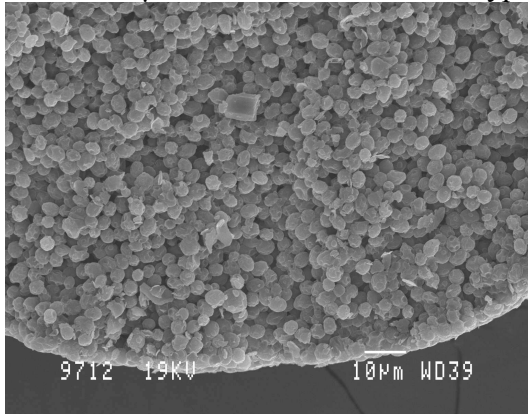


Figure 5 : Typical ESEM photography of a part of a yeast grain.

ESEM as well as mercury porosimetry only gives approximate results. Indeed, ESEM only offers surface analysis while mercury porosimetry can be damaging for the living structure of the yeast. Anyway, good agreement between both methods allows to use the 15 μm pore diameter as an average value.

Throat size is evaluated considering that flow limitation will occur where 3 colonies are close to each others, presenting structure comparable to those of dense packing.

So, a mean equivalent throat radius of 35 % of the grain radius can be assumed (Bryant and Blunt, 1992). Uniform distribution around this mean value is chosen for simplicity purpose. Maximum variation of 20% is chosen based on a rough estimation of distributions obtained for sphere packing by Nolan and Kavanagh (1994).

The magnitude of film flow cannot be investigated. Therefore the film hydraulic conductivity κ is taken as fitting parameter.

2.5. Shrinking core model

For comparison purpose, a continuous model for fluidized bed drying, simpler than the porous network, is presented. Details of this model can be found elsewhere (Debaste et al., 2007). This model assumes 2 steps in the drying. The first one is evaporation of water from the surface of the solid, highlighting a constant drying rate. The second one, corresponding to falling rate period, assumes that the liquid forms an uniform receding front in the material. Mass transfer limitation is then due to diffusion in the dry part of the solid structure.

Equations of the shrinking core model are the same as equations (14) and (15). Only the evaluation of evaporation rate is different. For the constant rate period, it writes as

$$\frac{dx}{dt} = -ka \left(\frac{p_{sat}(T)}{RT} - \frac{p_g}{RT} \frac{y}{\frac{M_v}{M_g} + y} \right) M_v \quad (16)$$

where k is the mass transfer coefficient, evaluated using classical correlations, see Ranz and Marshal (1952) for example.

On the other hand, for falling rate period, expression becomes

$$\left(\frac{1}{k} + \frac{1}{k_i} \right) \frac{dx}{dt} = -a \left(\frac{p_{sat}(T)}{RT} - \frac{p_g}{RT} \frac{y}{\frac{M_v}{M_g} + y} \right) M_v \quad (17)$$

where k_i take into account the diffusionnal resistance in the porous medium and is expressed as a function of water content :

$$k_i = \frac{D\varepsilon}{\tau} \frac{1}{\sqrt{\frac{x_{cri} - x_{res}}{x - x_{res}} - 1}} \quad (18)$$

where x_{cri} is the critical humidity, corresponding to the end of the constant rate drying, x_{res} is the residual humidity at the end of the drying, ε and τ are the grain porosity and tortuosity. This last parameter has no precise experimental value. Therefore, it is used as fitting parameter for the model.

3. Results and Analyses

3.1. Validation of porous network models on TGA experiment

The complete porous network model previously presented, coupled with energy equation (14) is used. The 2D network corresponding to a vertical slice of the sample is made of 17100 pores. Full computation time on a recent workstation for a model coded in Matlab is about 24 hours.

Figure 6 presents the comparison between experimental results and the model for a constant value of film hydraulic conductivity $\kappa = 0.005$. Even if instantaneous values don't really match, global dynamic is well reproduced. For the initial period, the discrepancy with experiment probably relies on the fact that the model doesn't take into account all the dynamic of the experiment start. At the end also, the model predicts a totally different end of drying. For the last percent of humidity porous media structure has an important impact on the kinetic and the drastic assumptions made on network topology aren't satisfactory anymore.

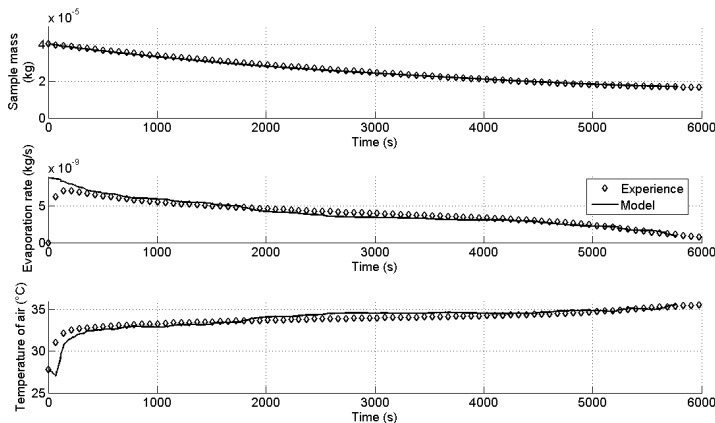


Figure 6: Comparison between TGA experimental results and network model. The abscise presents the time evolved since the beginning of the experiment. From top to bottom total sample mass, outlet air humidity and outlet air temperature are presented

3.2. Application of the porous network model to fluidized bed drying

For this system, equations (14) to (15) are coupled to the network model.

The 2D network of a grain, corresponding to a slice of the 3D real geometry counts 3805 pores. A simulation of the drying of this geometry takes about half an hour on a recent workstation.

Figure 7 presents the comparison between experimental results and the model for the κ value fitted on TGA experiment. Major features of the drying are correctly predicted. Only the precise end of the constant rate period is not well simulated. Once again, this is due to the highly approximate description of the porous structure.

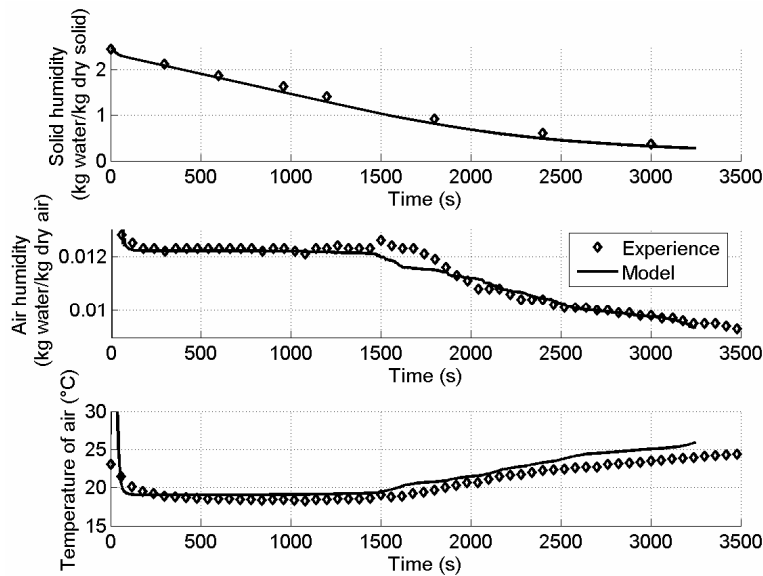


Figure 7 : Comparison between the porous network model results, expressed as the time evolution of solid humidity x , air humidity y and temperature T in the fluidized bed, and the corresponding experimental values.

With this model, a physical interpretation of the drying curve can be deduced. During of the whole process liquid front recedes in the grain. During the constant rate period films transport enough liquid to saturate the grain surface in vapor. In the falling rate period, films leave grains surface and drying is limited by vapor diffusion. This evolution is illustrated on Figure 8 where film thickness in the grain is mapped at different times. On the left, at the beginning of the drying, liquid is still close to the exterior and film saturates easily the grain surface. In the middle, just before the end of the constant rate period liquid is clearly more dispersed, film still saturates the surface. On the right, at the end of the drying, only a few filled pores remain and film isn't connected to the surface anymore.

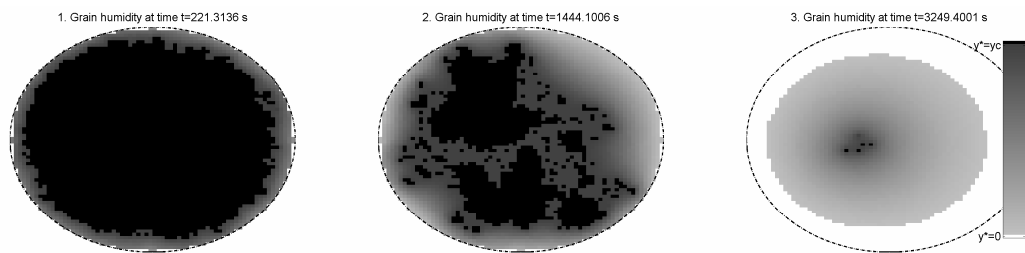


Figure 8 : Map of the film thickness in the grain at different time. Black correspond to liquid filled regions, gray scales correspond to film thickness and white zone to gas filled region. Dotted line represents grain surface.

3.3. Application of shrinking core model to fluidized bed drying

Equations from (14) to (18) are numerically solved with Mathematica. In Figure 9, the experimental results and the model predictions are compared. $\tau = 6$ is used. This value allows getting the best possible comparison between the numerical and

experimental values of the air humidity in the fluidized bed. It is obtained using the least square optimization method. A remarkable agreement is observed during the whole drying process. The model perfectly catches the dynamics of the experimental data. The change of concavity observed in the air humidity curve during the falling rate period is indeed well reproduced by the model.

It can be observed that the experimental temperature is slightly lower than the numerical one during the whole duration of the drying process, but especially during the falling drying rate period. This is attributed to heat loss through the uninsulated walls of the fluidized bed. This loss is not taken into account in the modelling work. Cross validation of the model on other experiments using the optimal τ values can be found in Debaste *et al* (2007).

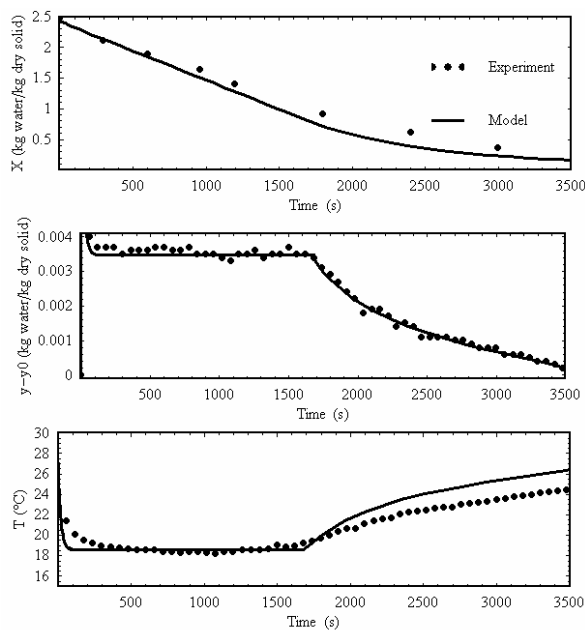


Figure 9 : Comparison between the shrinking core model results, expressed as the time evolution of solid humidity x , air humidity y and temperature T in the fluidized bed, and the corresponding experimental values. $\tau = 6$ is taken

4. Discussion and Conclusions

4.1. Network model

Network model gives acceptable results for both TGA and fluidized experiments. Difference of ambient humidity between the experiment setup induces different dominant phenomena for the drying. In the TGA experiment low vapor pressure next to the sample cause the transfer to be limited by vapor diffusion. In fluidized bed, high reactor vapor pressure allows development of film transport in the grain, corroborating the existence of a long constant drying rate phase.

Simulations reproduce the overall dynamic of the system but lack a precise fitting. This can be partially attributed to the highly coarse reproduction of the network topology. Exact coordination number is known not to be of critical importance but use of 2D network limits the capability of the system to simulate some dynamic effects (Blunt et al., 2002). The estimated pore and throat size distribution is also only a first draft. Future study, based on microtomography analysis (Al-Raoush and Willson, 2005) will tackle this problem.

4.2. Shrinking core model

This model is based on the assumption that drying is controlled by two successive mechanisms. The first one, evaporation from the surface is supposed to explain the existence of a constant drying rate period. The model cannot predict the duration of this step. Moreover, TGA experiment isn't controlled by the same limiting phenomena as fluidized bed, therefore, this model cannot correctly describe it.

Nevertheless, for cases where the limiting phenomena are included, this model becomes a powerful tool for process optimization. Main limitation is that the critical humidity isn't predicted by the model. Also, it is important to note that no grain shrinkage is taken into account. Its possible effects are hidden in the adjustable parameter τ .

4.3. Conclusion

Two different experimental setups were used to compare two modeling approaches: a porous network model and a simple shrinking core model. The two models offer complementary results. The shrinking core is a simple physical model that gives accurate results with small computational needs. The main limitation of this simple approach lies on the a priori assumption of limiting phenomena. On the other hand, the porous network is a complex model, with important computational needs. Obtaining precise results relies on a good knowledge of porous structure and topology. Presented network model is still far from producing a fully physical acceptable presentation of the porous structure, lots of assumptions were hidden in the adjustable parameter. Still, the model allows better understanding of limiting phenomenon in different experimental conditions therefore offering a more general application field than the shrinking core model. Hence, porous network can be used as a first general model to correctly spot possible assumptions for a simpler specific model, like the receding front one.

Nomenclature

a	solid specific surface (m^2 of external surface / kg of dry solid)
c_p	specific heat (J/kg/K)
d	throat specific diameter (m)
D	diffusion coefficient (m^2/s)
G	air mass flow rate on dry basis (kg/s)
k	mass transfer coefficient (m/s)
l	length of a throat (m)

m	mass (kg)
M_v	molecular mass of vapor (kg/mole)
p	pressure (Pa)
R	perfect gas constant (J/mole/°K)
t	time (s)
T	temperature (K)
x	water content (kg water/kg dry solid)
y	the film thickness (m)

Greek symbols

δ	external diffusion layer thickness (m)
Δ	laplacian operator.
ε	porosity
Φ	non dimensional variable defined in equation (6)
γ	interfacial tension (N/m)
κ	hydraulic conductivity coefficient
λ	water latent heat of vaporization (J/kg)
μ	viscosity of liquid (m ² /s)
ρ_l	volumetric mass of liquid (kg/m ³)
τ	tortuosity
Ω	throat cross section (m ²)

Subscripts

c	at liquid film interface
cri	critical
g	gas
in	at the reactor entrance
i,j	position indexes
l	liquid
res	residual
s	solid
sat	saturation
v	vapor

Superscripts

*	non-dimensionnal
-	average

Dimensionless numbers

Ca	capillary number
----	------------------

References

- Al-Raoush, R., and Willson, C. (2005) Extraction of physical realistic pore network properties from three-dimensional synchrotron x-ray microtomography images of unconsolidated porous media systems. *Journal of hydrology* 300, 44–64
- Bayrock, D., & Ingledew, W. M. (1997a). Fluidized bed drying of baker's yeast: moisture levels, drying rates and viability changes during drying. *Food Research International*, 30(6), 407 – 415.
- Bayrock, D., & Ingledew, W. M. (1997b). Mechanism of viability loss during fluidized bed drying of baker's yeast. *Food Research International*, 30(6), 417 – 425.
- Bear, J. & Buchlin, J.M. (1991) *Modelling and applications of transport phenomena in porous media*, volume 5 of *Theory and applications of transport in porous media*. Dordrecht: Kluwer Academic Publisher
- Bird, R. B., Stewart, W. E., & Lightfoot, E. N. (2002). *Transport phenomena*. New York: John Wiley & Sons, Inc.
- Blunt, M. J., Jackson, M., Piri, M., and Valvatne, P. (2002) Detailed physics, predictive capabilities and macroscopic consequences for pore-network models of multiphase flow. *Advances in water resources* 25, 1069–1090
- Bossart, L. (2006). Contribution à l'optimisation du séchage en lit fluidisé. PhD Thesis, Université Libre de Bruxelles
- Boulton, C., and Quain, D. (2001) *Brewing yeast and fermentation*. Blackwell Publishing
- Bryant, S., and Blunt, M. (1992) Prediction of relative permeability in simple porous media. *Physical Review A* 46, 4, 2004–2011
- Chen, X. D., and Patel, K. (2007) Micro-organism inactivation during drying of small droplets or thin slabs - a critical review of existing kinetics models and an appraisal of the drying rate dependent model. *Journal of Food Engineering* 82, 1–10.
- Debaste, F., Halloin, V., Bossart, L. & Haut, B. (2007). A new modeling approach for the prediction of yeast drying rates in fluidized beds. Accepted for publication in the *Journal of Food Engineering*.
- Laurindo, J., and Prat, M. (1996) Numerical and experimental network study of evaporation in capillary porous media. phase distributions. *Chemical engineering science* 51, 23, 5171–5185.
- Laurindo, J., and Prat, M. (1998) Numerical and experimental network study of evaporation in capillary porous media. drying rate. *Chemical engineering science* 53, 12, 2257–2269
- Le Bray, Y., and Prat, M. (1999) Three-dimensional pore network simulation of drying in capillary porous media. *International journal of heat and mass transfer* 42, 4207–4224
- Nolan, G., and Kavanagh, P. (1994) The size distribution of interstices in random packings of sphere. *Powder technology* 78, 231–238.
- Prat, M. (1995) Isothermal drying of non-hygroscopic capillary-porous materials as an invasion percolation process. *International journal of multiphase flow* 21, 5, 875–892
- Prat, M. (2002) Recent advances in pore-scale models for drying of porous media. *Chemical engineering journal* 86, 153–164
- Ranz, W. E. & Marshall, W. R. (1952). Evaporation from drops, *Chemical Engineering Progress*, 48, 141-146
- Sahimi, M. (1993). Flow phenomena in rocks : from continuum models to fractals percolation, cellular automata, and simulated annealing. *Reviews of modern physics* 65, 4, 1393-1537.
- Türker, M., Kanarya, A., Yüzgeç, U., Kapucu, H. & Senalp, Z. (2006); Drying of baker's yeast in batch fluidized bed. *Chemical Engineering and Processing*, 45, 1019-1028.
- Versteeg, H., and Malalasekera, W. (1995) *An introduction to computational fluid dynamics*. Pearson-Prentice Hall.
- Whitaker, S. (1977) A theory of drying in porous media. *Advances in heat transfer* 13, 119–203
- Yiotis, A., Stubos, A., Boudouvis, A., and Yortsos, Y. (2001). A 2-d pore-network model of the drying of single-component liquids in porous media. *Advances in Water Resources* 24, 439–460.
- Yiotis, A., Boudouvis, A., Stubos, A., Tsimpanogiannis, I., and Yortsos, Y. (2004) Effect of liquid films on the drying of porous media. *AIChE Journal* 50, 11, 2721–2737

Acknowledgement

F. Debaste acknowledges financial support from the Fonds National de la Recherche Scientifique, Belgium